frontiers | Frontiers in Energy Research

TYPE Original Research
PUBLISHED 04 August 2023
DOI 10.3389/fenrg.2023.1235467

OPEN ACCESS

EDITED BY
Srete Nikolovski,
Josip Juraj Strossmayer University of Osijek, Croatia

REVIEWED BY
Yushuai Li,
University of Oslo, Norway
Adel Oubelaid,
Université de Bejaia, Algeria

*CORRESPONDENCE
Xinxin Lv,
xinxinlvhhuc@163.com

RECEIVED 06 June 2023
ACCEPTED 19 July 2023
PUBLISHED 04 August 2023

CITATION
Huang T and Lv X (2023), Load frequency control of power system based on improved AFSA-PSO event-triggering scheme.
Front. Energy Res. 11:1235467.
doi: 10.3389/fenrg.2023.1235467

Load frequency control of power system based on improved AFSA-PSO event-triggering scheme

Tenghao Huang and Xinxin Lv*

School of Information Science and Engineering, Zhejiang Sci-Tech University, Hangzhou, China

Aiming at the impact of redundant information transmission on network resource utilization in current power systems, an improved event-triggered scheme based on particle swarm optimization and artificial fish swarm algorithm for power system load frequency control (LFC) with renewable energy is proposed. First of all, to keep the stability and security of power systems with renewable energy, the load frequency control scheme is investigated in this paper. Then, to relieve the communication burden and increase network utilization, an improved event-triggered scheme based on the particle swarm algorithm and artificial fish swarm algorithm is explored for the power system load frequency control. Then, by utilizing improved Lyapunov functional and the linear matrix inequality method, sufficient condition for the H_∞ stability of the load frequency control system is established. Finally, a two-area load frequency control system and IEEE-39 node simulation models are constructed to verify the effectiveness and applicability of the proposed method.

KEYWORDS

event-triggered scheme, LFC systems, particle swarm optimization, artificial fish swarm algorithm, IEEE-39 node simulation models

1 Introduction

In the context of global clean energy and low-carbon development, environmental protection issues have gained increasing attention from numerous countries in recent years. Conventional power generation technologies' defects in the economy and environmental protection have become more prominent (Liu et al., 2021). Meanwhile, several new problems affecting the stable operation of power systems have arisen due to the rapid development of clean energy generation technology. For instance, new energy power systems are often subject to interruptions or fluctuations in power supply (Gholamrezaie et al., 2018; Oubelaid et al., 2022a). Energy storage technology is then applied to solve the technical deficiencies of the system power supply and ease the instability of the new energy power system (Oubelaid et al., 2022b). Therefore, the power system combines with a growing number of renewable energy sources and battery storage (Choi et al., 2016; Mi et al., 2017; Pulazza et al., 2021; Oubelaid et al., 2022c). However, environmental variations can have a significant impact on the output of renewable energy sources, leading to fluctuations in the power system's output power after the integration of renewable energy. Therefore, ensuring the maintenance of the load frequency within a safe range becomes particularly crucial after the integration of renewable energy sources into the power grid (Yan et al., 2022). Hence, the system needs a control strategy for regulation. As the core application of automatic power generation

control in power systems, load frequency control (LFC) is also an essential tool for dealing with grid frequency matters resulting from load changes (Zhao et al., 2022; Sun et al., 2023). LFC mainly adjusts the grid frequency deviation and the exchange power value of the contact line to make the system frequency reach the rated value, while maintaining the tie-lines exchanged power at the normal value (Yang et al., 2020).

It is worth mentioning that traditional LFC technology usually uses a dedicated line communication method to transmit data (Wang et al., 2022), with the drawbacks of high maintenance costs and poor flexibility. The last few decades have witnessed a spurt of progress in communication, computer, and control technology. Thus, this traditional method of communication is gradually being replaced by open networks (Aluko et al., 2021). However, the application of open communication networks in power systems has brought new problems such as communication delays and limited network bandwidth constraints (Yuan et al., 2021). Therefore, how to improve the utilization of network resources has been the focus of investigation on the power system in the modern communication network environment. It is worth noting that event-trigger scheme can effectively relieve bandwidth pressure (Li M. et al., 2019; Zhang et al., 2020).

In an event-trigger scheme, the event generator will only release the data packet signal while the preset event-trigger conditions are satisfied. Therefore, the event-triggered scheme is adopted in modern power systems to achieve the expected goal of saving the occupancy of communication channels (Wen et al., 2016). Based on the event-triggered scheme, LFC has received considerable attention in the power system. In (Bu et al., 2022), an event-triggered data-driven LFC scheme via model-free adaptive control is proposed, which achieves better data-driven linear frequency regulation based on an event-triggered scheme and dynamic linearization technique. In (Hossain et al., 2022), a distributed event-trigger scheme has been applied, whose triggering conditions depend on output information for specific regions. It is noteworthy that the performance of the event-trigger scheme is related to the trigger threshold, however, In the design of the event-trigger scheme in the above research results, the performance of the trigger scheme has been limited since the trigger threshold is required to be preset in advance (Wu et al., 2018). In consideration of the above situation, various research scholars have applied adaptive event-trigger schemes (Chen et al., 2022) to the study of power systems. For example, an adaptive event-trigger scheme for multi-area power systems with communication bandwidth constraints is designed (Peng et al., 2018). Consequently, the system can adaptively adjust the threshold parameters based on current and past data; the dynamic event-trigger scheme and adaptive event-trigger scheme for networked power systems are investigated (Wu et al., 2020). The trigger parameters of the dynamic scheme are the upper limit of the trigger parameters of the adaptive scheme, both of which work together to balance the system control performance and the number of transmitted signals (Shangguan et al., 2022). Even though there have been many research results on the LFC event-triggered scheme, little research has been conducted on the optimal design of the event-trigger scheme.

Artificial fish swarm algorithm (AFSA) is a class of swarm intelligence optimization algorithms based on fish activity behavior (Tang et al., 2021). The algorithm has the ability of distributed processing as well as strong robustness of parameters and initial values (Lin et al., 2020; Yang et al., 2022). Particle swam optimization (PSO) is an algorithm inspired by the predatory behavior of birds and used to solve optimization problems (Tang et al., 2021; Belaid et al., 2022). The velocity of a particle is dynamically adjusted by its own and its companion's flight experience, thus enabling the individual to search in the solvable space. It is rather remarkable that AFSA has a strong global search capability, but the algorithm converges slowly at a later stage (Zhu and Gao, 2020). In contrast, PSO has the capability of local fast convergence but tends to fall into the local optimum (Dashtdar et al., 2022). This paper presents a hybrid AFSA-PSO algorithm, to make the merits and demerits of the two algorithms complementary, thereby addressing the optimization problem better. AFSA uses an adaptive vision and step size which can dynamically regulate the operating speed of the algorithm. Additionally, the introduction of the compression factor and adaptive inertia weight to PSO ensures the convergence of the algorithm and removes the boundary restriction on the velocity, resulting in a more satisfactory solution.

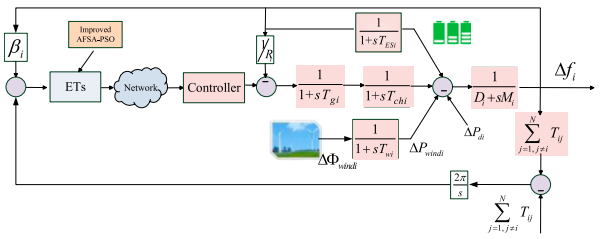

FIGURE 1
The structure of *i*-th area LFC.

Accordingly, to enhance the network bandwidth utilization, and reduce the transmission of redundant information for power system, this paper offers an improved event-triggered LFC based on a hybrid AFSA-PSO algorithm.

In consideration of the above discussions, this paper investigates a multi-area power system LFC based on the AFSA-PSO event-triggered scheme. The main contributions of this work are displayed below:

1) Since network communication is constrained by limited network bandwidth, this paper introduces an event-trigger scheme. The specific form of performance is to improve the utilization of network resources and ease the pressure on communication bandwidth by screening the measured output signal of the LFC power system. In the meantime, a hybrid AFSA-PSO algorithm is proposed to optimize the parameters that determine the threshold conditions in this paper, leading to the improved performance of the event-trigger scheme. AFSA is employed early in the method, and PSO has applied afterward, which makes the algorithm have high solution accuracy and convergence speed. In addition, this paper also optimizes and improves the AFSA and PSO respectively, to enable the algorithm to attain better performance.
2) The conservatism of the stability criterion design process is reduced under improved Lyapunov function. On the one hand, an improved Lyapunov function is constructed in the stability-proof process. On the other hand, the utilization of the double B-L inequality in the inequality scaling process decreases the conservatism of the resulting criterion.

TABLE 1 LFC symbol description of the multi-area power system.

Symbol	Description
ΔP_{di}	Load deviation
ΔP_{mi}	Generator mechanical output deviation
ΔP_{vi}	Valve position deviation
Δf_i	Frequency deviation
M_i	Moment of inertia
D_i	Generator damping coefficient
T_{gi}	Time constant of the governor
T_{chi}	Time constant of the turbine
R_i	Speed drop
β_i	Frequency bias factor
T_{ij}	Tie-line synchronizing coefficient

2 Problem statement

2.1 Describe of LFC model

For multi-area power systems, the LFC system structure of the i-th area can be shown in Figure 1. The parameters of i-th control area are listed in Table 1.

The multi-area power system dynamics LFC model studied in this paper can be described as:

$$\begin{cases} \dot{x}(t) = Ax(t) + Bu(t) + F\omega(t) \\ y(t) = Cx(t) \end{cases} \tag{1}$$

where:

$$x_i(t) = \left[\Delta f_i \;\; \Delta P_{mi} \;\; \Delta P_{vi} \;\; \Delta P_{windi} \;\; \Delta P_{Bi} \;\; \int ACE_i \;\; \Delta P_{tie-i}\right]^T$$
$$x(t) = \left[x_1{}^T(t) \;\; x_2{}^T(t) \;\; x_3{}^T(t) \;\; \ldots \;\; x_n{}^T(t)\right]^T$$
$$\omega_i(t) = \left[\Delta P_{di} \;\; \Delta\Phi_{windi}\right]^T, A_{ij} = \left[(7,1) = -2\pi T_{ij}\right]$$
$$u(t) = \left[u_1{}^T(t) \;\; u_2{}^T(t) \;\; u_3{}^T(t) \;\; \ldots \;\; u_n{}^T(t)\right]^T$$
$$y_i(t) = \left[ACE_i \;\; \int ACE_i\right]^T, B = diag\{B_1, .., B_n\}$$
$$\omega(t) = \left[\omega_1{}^T(t) \;\; \omega_2{}^T(t) \;\; \omega_3{}^T(t) \;\; \ldots \;\; \omega_n{}^T(t)\right]^T$$
$$y(t) = \left[y_1{}^T(t) \;\; y_2{}^T(t) \;\; y_3{}^T(t) \;\; \ldots \;\; y_n{}^T(t)\right]^T$$

$$A_{ii} = \begin{bmatrix} (1,1) = \dfrac{-D}{M_i}, (1,2) = \dfrac{1}{M_i}, (1,4) = \dfrac{1}{M_i}, \\ (1,5) = \dfrac{1}{M_i}, (1,7) = \dfrac{-1}{M_i}, (2,2) = \dfrac{-1}{T_{chi}}, \\ (2,3) = \dfrac{1}{T_{chi}}, (3,1) = \dfrac{-1}{RT_{gi}}, (3,3) = \dfrac{-1}{T_{gi}}, \\ (4,4) = \dfrac{-1}{T_{wi}}, (5,1) = \dfrac{1}{T_{ESi}}, \\ (5,5) = -\dfrac{1}{T_{ESi}}, (6,1) = \beta_i, \\ (6,6) = 1, (7,1) = 2\pi \sum_{j=1, j\neq i}^{n} T_{ij} \end{bmatrix}$$

$$A = \begin{bmatrix} A_{11} & \ldots & A_{1n} \\ \vdots & \ddots & \vdots \\ A_{n1} & \ldots & A_{nn} \end{bmatrix}$$
$$B_i = \begin{bmatrix} 0 & 0 & \left(\frac{1}{T_{gi}}\right)^T & 0 & 0 & 0 & 0 \end{bmatrix}^T$$
$$C_i = \begin{bmatrix} \beta_i & 0 & 0 & 0 & 0 & 0 & 1 \\ 0 & 0 & 0 & 0 & 0 & 1 & 0 \end{bmatrix}$$
$$F_i = \begin{bmatrix} \frac{-1}{M_i{}^T} & 0 & 0 & 0 & 0 & 0 & 0 \\ 0 & 0 & 0 & \frac{1}{T_{wi}} & 0 & 0 & 0 \end{bmatrix}^T$$
$$C = diag\{C_1, .., C_n\}, F = diag\{F_1, .., F_n\}$$

The Area Control Error (ACE) for each control area can be expressed by:

$$ACE_i = \beta_i \Delta f_i + \Delta P_{tie-i} \tag{2}$$

2.2 Design of improved event-triggered scheme

To save network bandwidth resources, and improve information transmission efficiency, an event-triggered scheme based on the improved AFSA-PSO algorithm is proposed to increase the utilization of network resources in this study. When the transmitted signal meets the trigger scheme, it may be transmitted; otherwise, the sampling signal will not be transmitted, and the event-triggered conditions are designed as follows (Yue et al., 2013):

$$\left[x(t_l h + jh) - x(t_l h)\right]^T \Phi \left[x(t_l h + jh) - x(t_l h)\right] > \beta x(t_l h)^T \Phi x(t_l h) \tag{3}$$

where, Φ is the positive definite weighting matrix; β is the event-triggered threshold in the range of $[0, 1)$; $t_l h$ denotes the most recent data transmission moment and $t_l h + jh$ is the current sampling moment.

The event trigger determines the transmission of the system state. Assuming that the data has been successfully transferred at time $t_l h$, the next trigger moment $t_{l+1} h$ is:

$$t_{l+1} h = t_l h + \min\Big\{jh \Big| \left[x(t_l h + jh) - x(t_l h)\right]^T \Phi \left[x(t_l h + jh) - x(t_l h)\right] > \beta x(t_l h)^T \Phi x(t_l h)\Big\} \tag{4}$$

Transmission delays are unavoidable due to the presence of communication networks. It is reflected in the trigger scheme as whether $x(t_l h)$ or $x(t_{l+1} h)$ is received first. Define $\tau(t)$ as the transmission delay between the event trigger and the zero-order device at moment $t_l h$, and the maximum value of $\tau(t)$ is $\tau_{\max}$. Define the error between the most recently transmitted data and the currently sampled data as $e_l(t)$. The event-trigger scheme is treated in two cases as follows:

(1) When $t_l h + h + \tau_{\max} \geq t_{l+1} h + \tau_{l+1}$, define $\tau(t) = t - t_l h$, $\tau(t) \in [\tau_l, (t_{l+1} - t_l)h + \tau_{l+1}]$, and $e_l(t) = 0$。
(2) When $t_l h + h + \tau_{\max} < t_{l+1} h + \tau_{l+1}$, the subintervals are discussed as follows:

$$\tau(t) = \begin{cases} t - t_l h, k \in \Omega_0 \\ t - t_l h - nh, k \in \Omega_n \\ t - t_l h - jh, k \in \Omega_j \end{cases} \quad (5)$$

where,

$$\Omega_0 = [t_l h + \tau_l, t_l h + \tau_{\max})$$
$$\Omega_n = [t_l h + nh + \tau_{\max}, t_l h + nh + h + \tau_{\max})(n = 1, 2, .., j-1)$$
$$\Omega_j = [t_l h + jh + \tau_{\max}, t_{l+1} h + \tau_{l+1})$$

Thus, $e_l(t)$ can be written as:

$$e_l(t) = \begin{cases} 0, k \in \Omega_0 \\ x(t_l h) - x(t_l h + nh), k \in \Omega_n \\ x(t_l h) - x(t_l h + jh), k \in \Omega_j \end{cases} \quad (6)$$

where, $x(t_l h)$ is the most recent moment transmission data; $x(t_l h + nh)$ and $x(t_l h + jh)$ are the current moment sampling data, respectively.

Therefore, $y(t)$ can be rewritten as follows

$$y(t_l h) = Ce_l(t) + Cx(t - \tau_l(t)) \quad (7)$$

Remark 1: In this paper, a PSO with adaptive inertia weights (Li et al., 2019b) and compression factors (Zhou et al., 2019) are designed. This improved algorithm balances the local search and global search capability of PSO. Meanwhile, the boundary restriction on the conventional particle velocity is removed to ensure the convergence and accuracy of PSO. PSO can utilize the mechanism of sharing information among individuals in a group to make the whole solution process orderly. The core formula of the algorithm is given below:

$$v_i^d = \omega v_i^{d-1} + c_1 r_1 \left(pbest_i^d - x_i^d\right) + c_2 r_2 \left(gbest^d - x_i^d\right) \quad (8)$$

$$x_i^d = x_i^{d-1} + v_i^{d-1} t \quad (9)$$

Eq. 8 is the speed of the individual's step d, which consists of the speed inertia of the previous step itself ωv_i^{d-1}, the self-cognition part $c_1 r_1 (pbest_i^d - x_i^d)$, and the social cognition part $c_2 r_2 (gbest^d - x_i^d)$. Eq. 9 is the position of the individual at step d, which is determined by the position x_i^{d-1} at step $d-1$ and the velocity of step $d-1 \times$ time of motion, with the time of each step generally taken as 1. ω denotes the velocity inertia weight, c_1 denotes the individual acceleration factor, c_2 denotes the social acceleration factor, and r_1, r_2 are the random numbers on $[0, 1]$.

Where, $pbest_i^d$ represents the best position that the particle i has passed through by the end of the d iteration, and $gbest^d$ represents the best position that all particles have passed through. ω, c_1 and c_2 are important factors to be considered in optimizing the PSO. However, the traditional PSO usually sets these parameters to fixed values, making the algorithm unable to be dynamically adjusted according to the operation results. On the other hand, due to the fast information exchange between particles, the particles all move in the optimal direction and tend to be homogeneous, which tends to cause local convergence. This work proposes an improved PSO with the following formulations to address these defects.

$$v_i^d = \alpha\left[\omega_i^d v_i^{d-1} + c_1 r_1 \left(pbest_i^d - x_i^d\right) + c_2 r_2 \left(gbest^d - x_i^d\right)\right] \quad (10)$$

The algorithm is designed with adaptive inertia weights ω_i^d, whose value can change with the change of the fitness value. Take the problem of minimizing the degree of adaptation as an example: the smaller the current degree of adaptation, the closer to the optimal solution, the more local search is needed, and accordingly, the inertia weights become smaller; the larger the degree of adaptation, the farther away from the optimal solution, the more global search is needed, which requires a larger value of inertia weights. The details are shown in the following formula:

$$\omega_i^d = \begin{cases} \omega_{\min} + (\omega_{\max} - \omega_{\min}) \dfrac{f(x_i^d) - f_{\min}^d}{f_{average}^d - f_{\min}^d}, f\left(x_i^d\right) \le f_{average}^d \\ \omega_{\max}, f(x_i^d) > f_{average}^d \end{cases} \quad (11)$$

Individual learning factor c_1 and social (group) learning factor c_2 indicate information exchange among the particle swarm. A bigger value of c_1 causes the particles to seek too much within their local range, whereas a larger value of c_2 causes the particles to converge on the local optimum too soon. The flight speed of the particles is also hard to select. To effectively control the flight speed of particles and achieve an effective balance between global search and local search, this algorithm introduces a compression factor. The convergence of the PSO algorithm can be guaranteed by selecting the appropriate parameters. Taking $c_1 = c_2 = 2.05$, $C = c_1 + c_2 = 4.1$. The specific expression of the compression factor is listed as follows:

$$\alpha = \frac{2}{\left|\left(2 - C - \sqrt{C^2 - 4C}\right)\right|} \quad (12)$$

In conclusion, the simultaneous introduction of adaptive inertia weights and compression factors can effectively improve the search capability and convergence accuracy of PSO, thus enhancing PSO performance.

Remark 2: In addition, an AFSA with an adaptive field of view and step size (Yuan and Yang, 2019) is designed in this paper. The algorithm can adaptively adjust the field of view and step length of the fish, which can enhance the global search ability in the early stage of the algorithm and accelerate the convergence speed in the late stage of the algorithm. The AFSA is a swarm intelligence stochastic optimization algorithm, in which the artificial fish self-renew by behavior such as prey, swarm, and follow, thus achieving the optimal search. However, the traditional AFSA involves the concept of the field of view in which the selection of viewpoints is random and the step length of movement is also random, which not only causes a lot of wasted computation time but also affects the search speed and accuracy. Given this, this paper presents the adaptive field of view factor γ, and step size adjustment factor m_1. Through γ, the algorithm can purposefully adjust the field of view each time. In the initial stage of the algorithm, a large field of view is given to the prey behavior, and the field of view is gradually reduced as the iteration of the algorithm proceeds. On the other hand, a too small field of view in the later stages of the algorithm may lead to a smaller probability of searching for the global optimal solution. Therefore, when the number of iterations of the algorithm exceeds half, the reduction of the field of view is stopped so that it remains half of the initial value (the lower limit of the parameter field of view value can be set according to the specific problem). The expression is shown below:

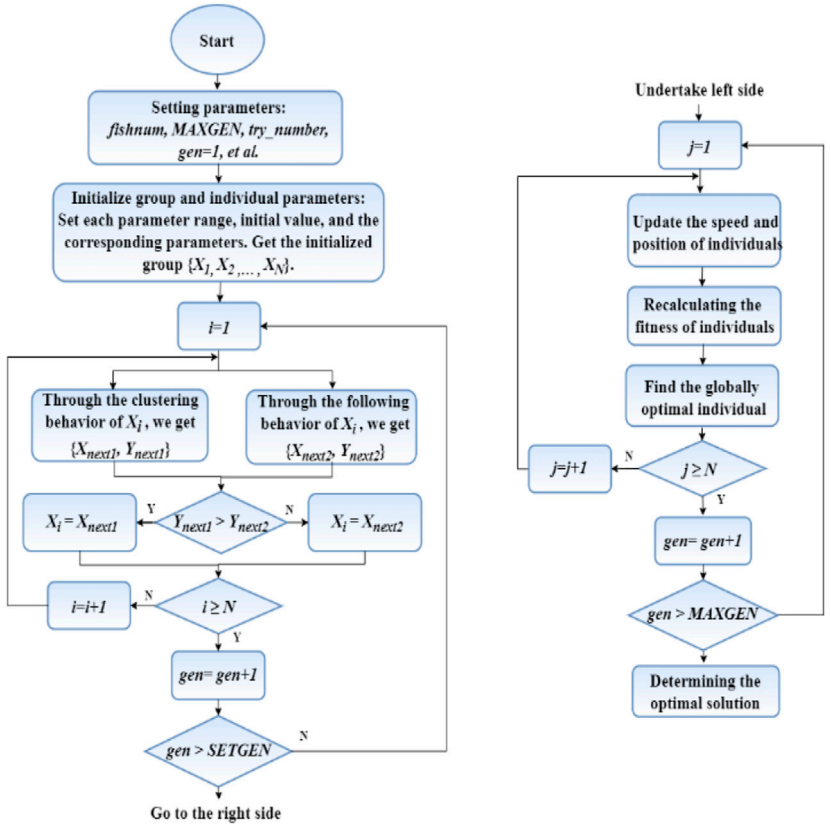

FIGURE 2
Flowchart of AFSA-PSO in optimizing event-triggered scheme.

$$\gamma_i^d = \begin{cases} \gamma_{\min} + (\gamma_{\max} - \gamma_{\min}) \dfrac{f(x_i^d) - f^d_{\min}}{f^d_{average} - f^d_{\min}}, f(x_i^d) \le f^d_{average} \\ \gamma_{\max}, f(x_i^d) > f^d_{average} \end{cases} \tag{13}$$

$$\begin{cases} vision_i^d = \gamma_i^d vision_0, d \le \dfrac{N}{2} \\ vision_i^d = \lambda vision_0, d > \dfrac{N}{2} \end{cases} \tag{14}$$

where, d is the current number of iterations of the algorithm, γ_i^d is the adaptive field of view factor, λ is the lower limit of the field of view factor, whose value is set according to the actual situation, N is the maximum number of iterations of the algorithm, $vision_0$ is the initially selected field of view value, and $vision_i^d$ is the field of view value obtained in this iteration.

The step size is similar to the selection of the field of view, which needs to be selected adaptively according to the fish population and concentration distribution. Therefore, as shown in (15), this paper introduces the step size adjustment factor, which enables the step size to be adjusted depending on the change in the field of view. Meanwhile, the step of redefining the step size is eliminated, and the algorithm becomes more concise.

$$step_i^d = m_1 vision_i^d \tag{15}$$

Remark 3: It is worth noting that AFSA has a strong global search capability, but the algorithm converges slowly at a later stage; PSO has a local fast convergence capability and can obtain a more accurate solution by adjusting the parameters, but it is easy to fall into a local optimum. Even though the two algorithms have been optimized separately, the above mentioned defects are still difficult to eliminate, which allows the introduction of hybrid optimization algorithms (Veerasamy et al., 2020). The algorithm proposed in this paper combines AFSA and PSO, which can combine the good characteristics of the two basic algorithms (Tsai and Lin, 2011). AFSA is applied in the early stage of the algorithm to expand the search range of individual best position and group best position, and PSO is utilized in the later stage of the algorithm to achieve a fine step-by-step search. It is proved that the algorithm can improve the convergence speed and solution accuracy to a certain extent.

Remark 4: Using disturbance attenuation level γ as the objective function, we obtain the optimal event-trigger threshold λ. The steps of the AFSA-PSO are shown below:

Step 1: Set parameters: such as fishnum(number of artificial fish),MAXGEN(maximum number of iterations), try_number(maximum number of tries), gen = 1(current number of iterations), etc.,; Initialize the population and individual parameters: set the range of each parameter, assign initial values to variables,

TABLE 2 Simulation parameters of the numerical example.

	T_p/s	T_T/s	T_G/s	T_{ES}/s
Area 1	10	0.3	0.1	0.038 2
Area 2	8	0.4	0.17	0.038 2
	K_p	R/(Hz/Mw)	K	β
Area 1	1	0.05	1	24
Area 2	0.667	0.05	1	24

form the population from the random array generated in the given range, set inertia weights, compression factors, control coefficients, etc.,;

Step 2: Start iteration, when the number of iterations is less than the preset value, the AFSA is used, otherwise the PSO is used;

Step 3: When the AFSA is used, the following operations are performed for each individual: set the adaptive field of view and step size, compare the fitness after performing following and swarming behaviors respectively, and keep the better fitness, then compare it with the individual optimum and population optimum, and update the fitness value;

Step 4: When the PSO is used, the following operations are performed for each individual: update the adaptive inertia weights, calculate the speed and position of the individual combined with the compression factor, recalculate the fitness value of the individual, find the global optimal individual, and update the optimal position of the individual and the group;

Step 5: Stop iteration when the maximum number of iterations is reached, and the obtained is the optimal solution.

Figure 2 can show the implementation of the code.

3 Stability analysis of multi-area LFC

In this section, an improved Lyapunov function and the B-L inequality are applied to study the stability criteria for the multi-area LFC with the improved event-triggered scheme (Lv et al., 2020).

Lemma 1: (Peng and Zhang, 2016): For a given positive matrix $R>0$, and differentiable function $\{\varphi(u)|u\in[a,b]\}$, the following inequality holds:

$$\int_a^b\int_\beta^b \dot{\varphi}^T(\alpha)R\dot{\varphi}(\alpha)\mathrm{d}\alpha\mathrm{d}\beta \geq 2\Omega_1^T R\Omega_1 + 4\Omega_2^T R\Omega_2 \tag{16}$$

$$\int_a^b\int_a^\beta \dot{\varphi}^T(\alpha)R\dot{\varphi}(\alpha)\mathrm{d}\alpha\mathrm{d}\beta \geq 2\Omega_3^T R\Omega_3 + 4\Omega_4^T R\Omega_4 \tag{17}$$

where:

$$\Omega_1 = \varphi(b) - \frac{1}{b-a}\int_a^b \varphi(\alpha)\mathrm{d}\alpha$$

$$\Omega_2 = \varphi(b) + \frac{2}{b-a}\int_a^b \varphi(\alpha)\mathrm{d}\alpha - \frac{6}{(b-a)^2}\int_a^b\int_\beta^b \varphi(\alpha)\mathrm{d}\alpha\mathrm{d}\beta$$

$$\Omega_3 = \varphi(a) - \frac{1}{b-a}\int_a^b \varphi(\alpha)\mathrm{d}\alpha$$

$$\Omega_4 = \varphi(a) - \frac{4}{b-a}\int_a^b \varphi(\alpha)\mathrm{d}\alpha + \frac{6}{(b-a)^2}\int_a^b\int_\beta^b \varphi(\alpha)\mathrm{d}\alpha\mathrm{d}\beta$$

The stability of the system (1) without disturbances will then be presented. The system (1) can be described as follows:

$$\dot{x}(t) = Ax(t) - BKCe(t) - BKCx(t-\tau(t)) \tag{18}$$

Theorem 1: For given positive d, τ_M, σ_m, the system (18) is asymptotically stable, if there exist positive definite matrices P, Q, R, S, Φ and appropriate dimensions X_1, X_2, X_3, X_4, such the following matrix inequalities hold:

$$\Pi_2 = \Pi_1 + \hat{H}_2\tilde{\varphi}_1\hat{H}_2^T + \varphi_3 + \varphi_4 + 2P\chi_1 + \chi_1\upsilon_2\chi_1^T < 0 \tag{19}$$

$$\tilde{\varphi}_1 = \begin{bmatrix} \varphi_1 & * \\ T_1 & \varphi_1 \end{bmatrix} > 0 \tag{20}$$

where:

$$\Pi_1 = e_1\upsilon_{1r}e_1^T - e_2\Phi e_2^T - e_3Q_2e_3^T - e_4\upsilon_3e_4^T$$

$$\upsilon_{1r} = Q_2 + \tau_M R_2,\ \upsilon_{2r} = d_M^2R_1 + \frac{d_M^2}{2}S_1 + \frac{d_M^2}{2}S_2$$

$$\upsilon_3 = (1-\dot{\tau}(t))Q_3 - \lambda(t_k h)\Phi$$

$$\tilde{\varphi}_2 = \begin{bmatrix} \varphi_{1r}+\tilde{S}_1 & * \\ T_1 & \varphi_{1r}+\tilde{S}_2 \end{bmatrix} > 0, \tilde{\varphi}_1 = \begin{bmatrix} \varphi_1 & * \\ T_1 & \varphi_1 \end{bmatrix},$$

$$H_1 = [e_1 - e_4 | e_1 + e_4 - 2e_5 e_1 - e_4 - 6e_6]$$

$$H_2 = [e_4 - e_3 | e_3 + e_4 - 2e_7 e_4 - e_3 - 6e_8], \hat{H}_2 = [H_1 H_2],$$

$$\varphi_1 = diag\{R_1, 3R_1, 5R_1\}, \tilde{S}_1 = diag\{S_1, 3S_1, 5S_1\}$$

$$\tilde{S}_2 = diag\{S_2, 3S_2, 5S_2\}, T_1 = \begin{bmatrix} T_{11} & T_{12} & T_{13} \\ T_{21} & T_{22} & T_{23} \\ T_{31} & T_{32} & T_{33} \end{bmatrix}$$

$$H_3 = \begin{bmatrix} e_1 - e_5 & e_1 - e_5 - 3e_6 & e_4 - e_7 & e_4 - e_7 - 3e_8 \end{bmatrix}$$

$$\varphi_3 = diag\{-2S_1, -4S_1, -2S_1, -4S_1\}$$

$$H_4 = \begin{bmatrix} e_5 - e_4 & e_4 - e_5 + 3e_6 & e_7 - e_3 & e_3 - e_7 + 3e_8 \end{bmatrix}$$

$$\varphi_4 = diag\{2S_2, 4S_2, 2S_2, 4S_2\}$$

$$\chi_1 = Ae_1 + BKCe_2 + BKCe_4$$

Proof: Defining the Lyapunov function as:

$$V(t) = V_1(t) + V_2(t) + V_3(t) + V_4(t)$$

$$V_1(t) = x^T(t)Px(t)$$

$$V_2(t) = \int_{t-\tau_M}^t x^T(s)Q_2x(s)ds + \int_{t-d(t)}^t x^T(s)Q_3x(s)ds$$

$$V_3(t) = d_M\int_{-d_M}^0\int_{t+\alpha}^t \dot{x}^T(s)R_1\dot{x}(s)ds\mathrm{d}\alpha + \int_{-d_M}^0\int_{t+\alpha}^t x^T(s)R_2x(s)ds\mathrm{d}\alpha$$

$$V_4(t) = \int_{-d_M}^0\int_\beta^0\int_{t+\alpha}^t \dot{x}^T(s)S_1\dot{x}(s)ds\mathrm{d}\alpha\mathrm{d}\beta + \int_{-d_M}^0\int_{-d_M}^\beta\int_{t+\alpha}^t \dot{x}^T(s)S_2\dot{x}(s)ds\mathrm{d}\alpha\mathrm{d}\beta$$

where: $P>0$, $Q>0$, $R>0$, $S>0$ are positive-definite matrices.

Calculating the derivate along the trajectory (18) yields the following inequality:

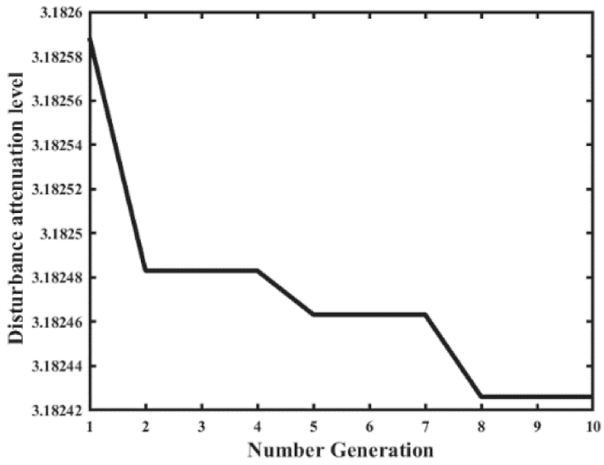

FIGURE 3
Optimizing algorithm performance.

$$\Delta V(t) = \Delta V(t)_1 + \Delta V(t)_2 + \Delta V(t)_3 + \Delta V(t)_4 \tag{21}$$

where:

$$\Delta V_1(t) = 2\dot{x}^T(t)Px(t)$$

$$\Delta V_2(t) = x^T(t)Q_2x(t) - x^T(t-d_M)Q_2x(t-d_M) + x^T(t)Q_3x(t) - \left(1-\dot{d}(t)\right)x^T(t-d(t))Q_3x(t-d(t))$$

$$\Delta V_3(t) = d_M^2\dot{x}^T(t)R_1\dot{x}(t) - d_M\int_{t-d_M}^{t}\dot{x}^T(\alpha)R_1\dot{x}(\alpha)d\alpha + d_Mx^T(t)R_2x(t) - \int_{t-d(t)}^{t}x^T(\alpha)R_2x(\alpha)d\alpha$$

$$\Delta V_4(t) = \frac{d_M^2}{2}\dot{x}^T(t)S_1\dot{x}(t) - \int_{-d(t)}^{0}\int_{t+\alpha}^{t}\dot{x}^T(s)S_1\dot{x}(s)dsd\alpha - \int_{-d_M}^{-d(t)}\int_{t+\alpha}^{t-d(t)}\dot{x}^T(s)S_1\dot{x}(s)dsd\alpha - (d_M-d(t))\int_{t-d(t)}^{t}\dot{x}^T(\alpha)S_1\dot{x}(\alpha)d\alpha + \frac{d_M^2}{2}\dot{x}^T(t)S_2\dot{x}(t) - \int_{-d(t)}^{0}\int_{t-d(t)}^{t+\alpha}\dot{x}^T(s)S_2\dot{x}(s)dsd\alpha - \int_{-d_M}^{-d(t)}\int_{t-d_M}^{t+\alpha}\dot{x}^T(s)S_2\dot{x}(s)dsd\alpha - d(t)\int_{t-d_M}^{t-d(t)}\dot{x}^T(s)S_2\dot{x}(s)ds$$

Defining the following augmenting state variable:

$$\xi(t) = [x(t) \quad e(t) \quad x(t-d_M) \quad x(t-d(t)) \quad \frac{1}{d(t)}\int_{-d(t)}^{0}x(t+\alpha)d\alpha \quad \frac{1}{d(t)}\int_{-d(t)}^{0}\lambda_{-\tau(t)}(\alpha)x(t+\alpha)d\alpha \quad \frac{1}{d_M-d(t)}\int_{-d_M}^{-d(t)}x(t+\alpha)d\alpha \quad \frac{1}{d_M-d(t)}\int_{-d_M}^{-d(t)}\lambda_{-\tau(t)}(\alpha)x(t+\alpha)d\alpha]$$

Thus, the next inequality can be obtained:

$$\Delta V(t) \le \xi(t)\Pi_1\xi^T(t) + 2\dot{x}(t)Px^T(t) + \dot{x}(t)v_2\dot{x}^T(t) + \Delta\tilde{V}_1(t) + \Delta\tilde{V}_2(t) + \Delta\tilde{V}_3(t)$$

where:

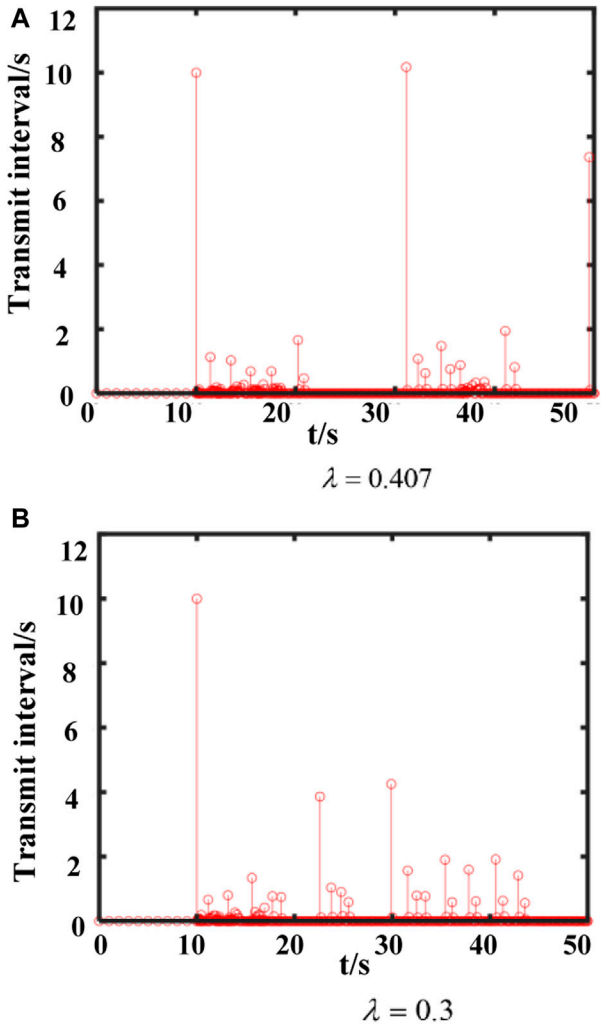

FIGURE 4
Release instant and release intervals.

$$\Delta\tilde{V}_1(t) = -d_M\int_{t-d_M}^{t}\dot{x}(s)R_1\dot{x}^T(s)ds - \left(d_M-\dot{d}(t)\right)\int_{t-d(t)}^{t}\dot{x}(s)S_1\dot{x}^T(s)ds - \dot{d}(t)\int_{t-d_M}^{t-d(t)}\dot{x}(s)S_2\dot{x}^T(s)ds$$

$$\Delta\tilde{V}_2(t) = -\int_{-d(t)}^{0}\int_{t+\alpha}^{t}\dot{x}(s)S_1\dot{x}^T(s)dsd\alpha - \int_{-d_M}^{-d(t)}\int_{t+\alpha}^{t-d(t)}\dot{x}(s)S_1\dot{x}^T(s)dsd\alpha$$

$$\Delta\tilde{V}_3(t) = -\int_{-d(t)}^{0}\int_{t-d(t)}^{t+\alpha}\dot{x}(s)S_2\dot{x}^T(s)dsd\alpha - \int_{-d_M}^{-d(t)}\int_{t-d_M}^{t+\alpha}\dot{x}^T(s)S_2\dot{x}(s)dsd\alpha$$

Applying the B-L inequality, $\Delta\tilde{V}_1(t)$ can be rewritten as:

$$\Delta\tilde{V}_1(t) \le -\frac{1}{\iota}\xi(t)H_1\left(\varphi_1+\tilde{S}_1\right)H_1^T\xi^T(t) - \frac{1}{\kappa}\xi(t)H_2\left(\varphi_1+\tilde{S}_2\right)H_2^T\xi^T(t) + \xi(t)H_1\tilde{S}_1H_1^T\xi^T(t) + \xi(t)H_2\tilde{S}_2H_2^T\xi^T(t) \le -\xi(t)\hat{H}_2\tilde{\varphi}_1\hat{H}_2{}^T\xi^T(t)$$

Applying Lemma 1, we obtain:

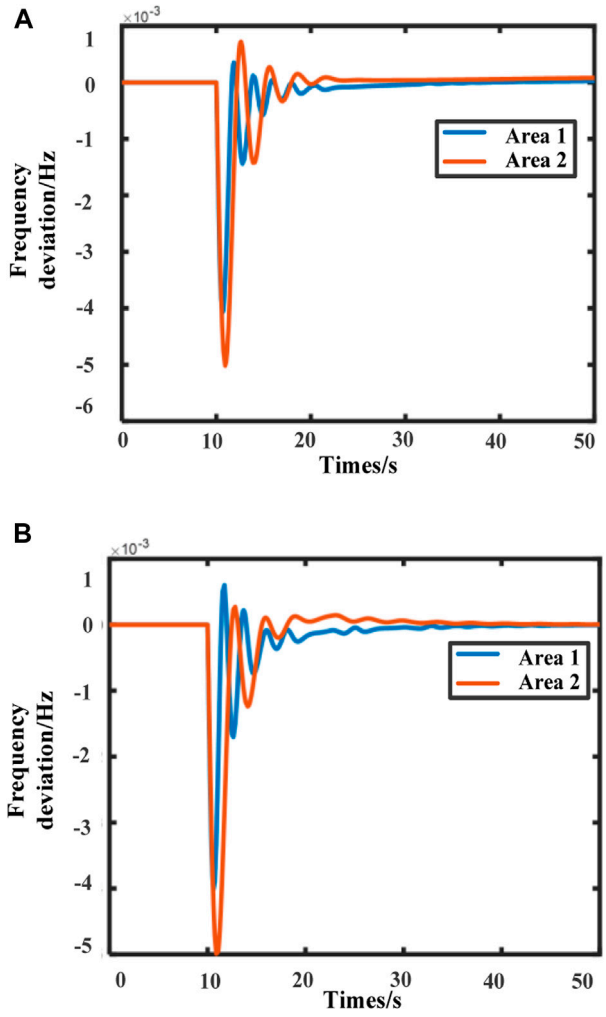

FIGURE 5
Frequency deviations of LFC power system.

$$\Delta\tilde{V}_2(t) \le H_3\varphi_{3r}H_3^T$$
$$\Delta\tilde{V}_3(t) \le -H_4\varphi_4H_4^T$$

Therefore, if $\tilde{\varphi}_2 = \begin{bmatrix} \varphi_1 + \tilde{S}_1 & * \\ T_1 & \varphi_1 + \tilde{S}_2 \end{bmatrix} > 0$ can be satisfied, the following result can be obtained:

$$\begin{aligned}\Delta V(t) \le{}& \xi(t)\Pi_1\xi^T(t) + 2\dot{x}(t)Px^T(t) + \dot{x}(t)\upsilon_2\dot{x}^T(t)\\ &+\Delta\tilde{V}_1(t) + \Delta\tilde{V}_2(t) + \Delta\tilde{V}_3(t)\\ \le{}& \xi(t)\Pi_2\xi^T(t)\end{aligned}$$

LMI (17) can be verified if $\Pi_2 < 0$ is satisfied and Lemma 1 is applied. Considering a sufficiently small scalar $c \in (0, 1]$, it is possible to verify that $\Delta V(t) < \xi(t)\Pi_2\xi^T(t) < -c\|\xi(t)\|^2 < 0$. Therefore, according to Theorem 1, the system (18) is stochastically stable. Theorem 1 provides the criterion of asymptotic stability. Next, the H_∞ stability criterion for the system (18) will be designed.

Theorem 2: For given positive constant γ, d, τ_M and σ_m, if there exist positive definite matrices P, Q, R, S, W, Φ and appropriate dimensions X_1, X_2, X_3, X_4, such the following matrix inequalities hold, the system (18) is asymptotically stable with H_∞ prescribed attenuation level γ.

$$\begin{aligned}\Pi_2' = \Pi_1 + \hat{H}_2\tilde{\varphi}_1\hat{H}_2^T + \varphi_3 + \varphi_4 + 2P\chi_1' + \chi_1'\upsilon_2\chi_1'^T\\ -\gamma^2e_{10}^Te_{10} + e_1^TC^TCe_1 < 0\end{aligned} \tag{22}$$

where:

$$\chi_1' = Ae_1 + BKCe_2 + BKCe_4 + Fe_9$$
$$e_j = \left[\underset{j-1}{0\ldots0}, 1, \underset{9-j}{0\ldots0}\right],\ (j = 1, \ldots, 9)$$

Proof: The proof of this theorem is based on Theorem 1. For the prescribed attenuation level $\gamma > 0$, the cost function J can be defined as:

$$J = \int_0^\infty y^T(t)y(t) - \gamma^2\omega^T(t)\omega(t)\mathrm{d}t \tag{23}$$

For $\omega(t) \in l_2[0, \infty]$, and $t > 0$, the next inequality we have:

$$J \le \int_0^\infty y^T(t)y(t) - \gamma^2\omega^T(t)\omega(t) + \Delta V(t)\mathrm{d}t \tag{24}$$

Considering the improved event-triggered scheme, if the following inequality hold, $J < 0$ can be satisfied,

$$\begin{aligned}&y^T(t)y(t) - \gamma^2\omega^T(t)\omega(t) + \Delta V(t)\\ &-e^T(t)\Phi e(t) + \lambda x^T(t - \tau(t))\Phi x(t - \tau(t)) < 0\end{aligned} \tag{25}$$

Defining the augmenting state variable:

$$\xi'(t) = [\,\xi(t)\ \ \omega(t)\,]$$

For

$$\begin{aligned}\Omega^1 = {}& y^T(t)y(t) - \gamma^2\omega^T(t)\omega(t) + \Delta V(t)\\ &-e^T(t)\Phi e(t) + \lambda x^T(t - \tau(t))\Phi x(t - \tau(t))\end{aligned}$$

it yields:

$$\Omega^1 = \xi^T(t)\Pi_2'\xi'(t) \tag{26}$$

Thus, Theorem 2 is proved. The stability with H_∞ prescribed attenuation level γ of the system (18) is obtained.

From the above discussion, it is clear that to maintain a better stable performance and obtain a better event-triggered scheme, the attenuation level γ is necessary to minimize. By optimizing with AFSA-PSO, we can get the desired event-triggered threshold.

4 Case studies and discussion

In this section, two simulation examples are carried out to verify the performance of the proposed event-triggered LFC based on an improved AFSA-PSO. In this section, the two-area LFC system model as well as the IEEE-39 node system model are built using Simulink. Among them, the parameters of the two-area system model are shown in Table 2.

4.1 Two-area LFC system simulation experiment

Since the thresholds of different event-triggered schemes in LFC systems can have an impact on the system's performance. Therefore, this simulation experiment uses the hybrid AFSA-PSO to optimize the event-triggered scheme threshold with the system performance as the optimization objective. The process between the number of algorithm iterations and the optimized performance is shown in

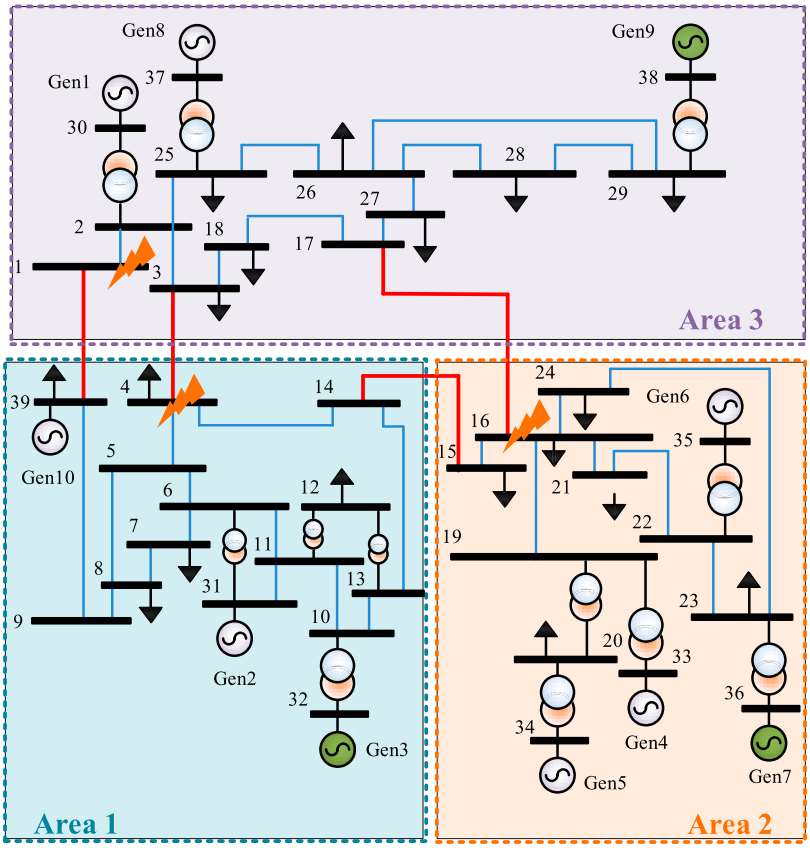

FIGURE 6
IEEE-39 bus test system.

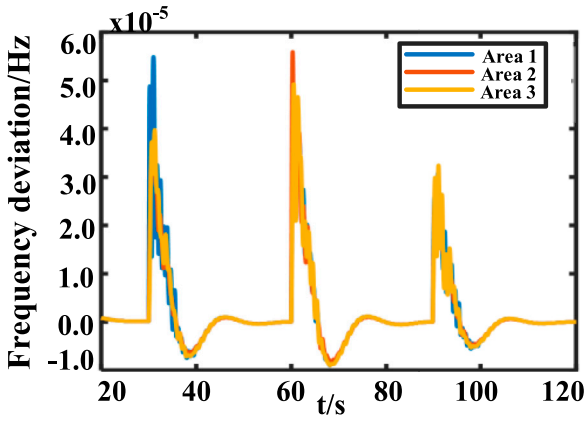

FIGURE 7
Frequency deviations of IEEE-39 bus test system.

Figure 3. Meanwhile, this experiment takes the two-area LFC system as the object and adds $\Delta P_d = 2Hz$ perturbations to Area 1 and Area 2 respectively when the system runs to 10s, to verify the LFC performance under the designed event-triggered scheme.

Based on the data presented in Figure 3, it is evident that the system's target value converges to a constant value of 3.18243 after eight iterations of the algorithm. Consequently, selecting the trigger threshold λ as 0.407 results in the minimization of the optimal attenuation level γ to 3.18243. Figure 4A displays the data release time and the interval of the two-area LFC system under the optimal attenuation level $\gamma = 3.18243$ and the triggered threshold $\lambda = 0.407$.

To assess the performance of the proposed event-triggered scheme, Figure 4B presents the release time and interval of data for the LFC system in two areas with the trigger threshold $\lambda = 0.3$. The figure indicates that the system functions normally and releases a relatively small amount of data between 0 and 10 s. However, when the system experiences disturbances, its performance is adversely affected, leading to the release of a significant amount of data. From the comparison of Figure 4A and Figure 4B, it can be seen that when the threshold value of the event-triggered scheme is 0.407, the amount of data released is less, which reduces the system performance loss as well as increases the network resource utilization.

To verify the performance of the LFC under the designed event-triggered scheme, the frequency deviation response plots of the system under the two event-triggered schemes are given separately, as shown in Figure 5. Figures 5A, B show the system frequency deviation Δf response curves when the system suffers a load deviation perturbation at $\lambda = 0.407$ as well as $\lambda = 0.3$, respectively. As can be seen from Figure 5, the Δf response can converge to zero in a short period when the system suffers a load

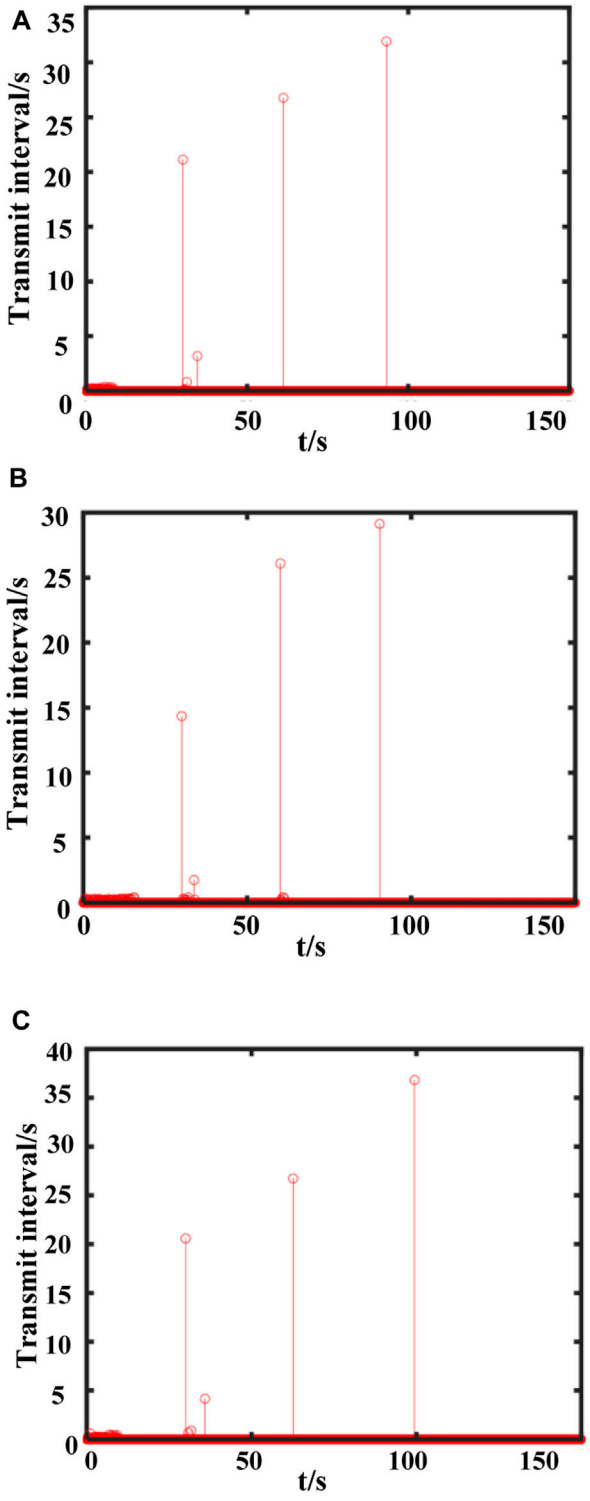

FIGURE 8
Release instant and release intervals of IEEE-39 bus test system.

disturbance at 10s. In addition, when $\lambda = 0.407$, the Δf response has a small overshoot and a short stabilization time. Therefore, the hybrid AFSA-PSO based event-triggered scheme designed in this paper has a better performance in reducing the amount of redundant information transmission. At the same time, the LFC system has better robustness to external disturbances under this event-triggered scheme.

4.2 IEEE-39 node system

In this simulation experiment, an IEEE-39 node model is built using MATLAB/Simulink. The model contains 10 diesel generators along with 19 loads and 34 transmission lines (Shangguan et al., 2022). Also, to verify the performance of the proposed LFC based on the improved event-triggered scheme, the system is divided into three control areas, with Gen3 as the selected generator in Area 1, Gen7 as the selected generator in Area 2, and Gen9 as the selected generator in Area 3. Figure 6 shows the schematic diagram of the IEEE-39 bus test system and the division of the control area.

At $t = 30s$, a 0.038p.u. Perturbation is added to node 8; at $t = 60s$, a 0.064p.u. Perturbation is added to node 16; at $t = 90s$, a 0.038p.u. Perturbation is added to node 3. At this time, the Δf response in the three areas and the trigger interval and trigger time in the event-triggered scheme are shown in Figure 7 as well as Figure 8.

From Figure 7 and Figure 8, it can be seen that the frequency deviation Δf in the three areas converges to a steady state within a short period when load perturbations are added to the three areas at $t = 30s$, $t = 60s$ and $t = 90s$, respectively. Figures 8A–C show the release instant and release intervals of the three areas, respectively. Meanwhile, at the moment of the perturbation, the system performance needs a large amount of data for improvement, and it can be seen from Figure 7 that the event-triggered scheme transmits a large amount of data at this time. And, as can be seen from Figure 8, the overshoot of the Δf response in the three areas is different at the three different moments of perturbation. At the moment of different disturbances, the generators responsible in the three areas respond to the load disturbance, and at the same time, the control errors between the areas deviate due to the interconnection between the areas, and the generating units in the remaining areas respond to the deviation of the exchange power between the areas. Therefore, the LFC with an improved event-triggered scheme designed in this paper has superior performance in the IEEE-39 node system.

5 Conclusion

To save network communication resources and reduce the information transmission frequency of multi-area power systems, this paper proposes an improved event-triggered scheme based on a hybrid AFSA-PSO and investigates LFC based on this scheme. In this paper, an LFC model with wind power and battery storage is established based on Markov theory. Based on this model, the stability of this system is studied by an improved Lyapunov function. Moreover, the conservatism of the resulting stability criterion is reduced by utilizing the double B-L inequality in the inequality scaling process. Compared with the traditional event-triggered scheme, the hybrid AFSA-PSO can optimize the threshold value rapidly and efficiently. The algorithm adopts the improved AFSA in the first stage and applies the improved PSO in the later stage, which can take into account the global and

local aspects of the search so that the algorithm has high solution accuracy and convergence speed. High performance event-triggered schemes obtained by optimizing event-triggered thresholds enable better frequency control while transmitting less information. In conclusion, this paper verifies the effectiveness of the improved event-triggered scheme in the two-area LFC system model as well as the IEEE-39 node system model.

Data availability statement

The original contributions presented in the study are included in the article/supplementary material, further inquiries can be directed to the corresponding author.

Author contributions

TH contributed to the conception of the study. The corresponding author XL is responsible for ensuring that the descriptions are accurate and agreed upon by all authors. All authors contributed to the article and approved the submitted version.

Conflict of interest

The authors declare that the research was conducted in the absence of any commercial or financial relationships that could be construed as a potential conflict of interest.

Publisher's note

All claims expressed in this article are solely those of the authors and do not necessarily represent those of their affiliated organizations, or those of the publisher, the editors and the reviewers. Any product that may be evaluated in this article, or claim that may be made by its manufacturer, is not guaranteed or endorsed by the publisher.

References

Aluko, A. O., (2021). Robust State Estimation Method for Adaptive Load Frequency Control of Interconnected Power System in a Restructured Environment. *IEEE Syst. J.* 15 (4), 5046–5056. doi:10.1109/jsyst.2020.3005979

Belaid, S., (2022). Proposed Hybrid Power Optimization for Wind Turbine/Battery System. *Periodica Polytech. Electr. Eng. Comput. Sci.* 66 (1), 60–71. doi:10.3311/ppee.18758

Bu, X., (2022). Event-Triggered Data-Driven Load Frequency Control for Multiarea Power Systems. *IEEE Trans. Ind. Inf.* 18 (9), 5982–5991. doi:10.1109/tii.2021.3130415

Chen, P., (2022). Dynamic Event-Triggered Output Feedback Control for Load Frequency Control in Power Systems With Multiple Cyber Attacks. *IEEE Trans. Syst. Man. Cybern. Syst.* 52 (10), 6246–6258. doi:10.1109/tsmc.2022.3143903

Choi, J. W., Heo, S. Y., and Kim, M. K. (2016). Hybrid Operation Strategy of Wind Energy Storage System for Power Grid Frequency Regulation. *IET Gener. Transm. Distrib.* 10 (3), 736–749. doi:10.1049/iet-gtd.2015.0149

Dashtdar, M., (2022). Improving the Power Quality of Island Microgrid With Voltage and Frequency Control Based on a Hybrid Genetic Algorithm and PSO. *IEEE Access* 10, 105352–105365. doi:10.1109/access.2022.3201819

Gholamrezaie, V., (2018). An Optimal Frequency Control Method Through a Dynamic Load Frequency Control (LFC) Model Incorporating Wind Farm. *IEEE Syst. J.* 12 (1), 392–401. doi:10.1109/jsyst.2016.2563979

Hossain, M. M., (2022). Bandwidth Allocation-Based Distributed Event-Triggered LFC for Smart Grids Under Hybrid Attacks. *IEEE Trans. Smart Grid* 13 (1), 820–830. doi:10.1109/tsg.2021.3118801

Li, M., (2019a). An Improved Particle Swarm Optimization Algorithm With Adaptive Inertia Weights. *Int. J. Inf. Technol. Decis. Mak.* 18 (03), 833–866. doi:10.1142/s0219622019500147

Li, Y., (2019b). Event-Triggered-Based Distributed Cooperative Energy Management for Multienergy Systems. *IEEE Trans. Ind. Inf.* 15 (4), 2008–2022. doi:10.1109/tii.2018.2862436

Lin, L., (2020). Deep Reinforcement Learning for Economic Dispatch of Virtual Power Plant in Internet of Energy. *IEEE Internet Things* 7 (7), 6288–6301. doi:10.1109/jiot.2020.2966232

Liu, Y., (2021). Automatic Generation Control for Distributed Multi-Region Interconnected Power System With Function Approximation. *Front. Energy Res.* 9. doi:10.3389/fenrg.2021.700069

Lv, X., (2020). Event-Triggered Load Frequency Control for Multi-area Power Systems Based on Markov Model: A Global Sliding Mode Control Approach. *IET Gener. Transm. Distrib.* 14 (21), 4878–4887. doi:10.1049/iet-gtd.2020.0186

Mi, Y., (2017). Sliding Mode Load Frequency Control for Multi-area Time-delay Power System With Wind Power Integration. *IET Gener. Transm. Distrib.* 11 (18), 4644–4653. doi:10.1049/iet-gtd.2017.0600

Oubelaid, A., (2022a). Fuzzy-Energy-management-based Intelligent Direct Torque Control for A Battery—Supercapacitor Electric Vehicle. *Sustainability* 14 (14), 8407. doi:10.3390/su14148407

Oubelaid, A., (2022b). Secure Power Management Strategy for Direct Torque Controlled Fuel Cell/Supercapacitor Electric Vehicles. *Front. Energy Res.* 10. doi:10.3389/fenrg.2022.971357

Oubelaid, A., Taib, N., and Rekioua, T. (2022c). Novel Coordinated Power Sources Switching Strategy for Transient Performance Enhancement of Hybrid Electric Vehicles. *COMPEL - Int. J. Comput. Math. Electr. Electron. Eng.* 41 (5), 1880–1919. doi:10.1108/compel-10-2021-0399

Peng, C., and Zhang, J. (2016). Delay-Distribution-Dependent Load Frequency Control of Power Systems With Probabilistic Interval Delays. *IEEE Trans. Power Syst.* 31 (4), 3309–3317. doi:10.1109/tpwrs.2015.2485272

Peng, C., Zhang, J., and Yan, H. (2018). Adaptive Event-Triggering ${H}_{\infty }$ Load Frequency Control for Network-Based Power SystemsH∞Load Frequency Control for Network-Based Power Systems. *IEEE Trans. Ind. Electron* 65 (2), 1685–1694. doi:10.1109/tie.2017.2726965

Pulazza, G., (2021). Transmission Planning With Battery-Based Energy Storage Transportation For Power Systems With High Penetration of Renewable Energy. *IEEE Trans. Power Syst.* 36 (6), 4928–4940. doi:10.1109/tpwrs.2021.3069649

Shangguan, X.-C., (2022). Control Performance Standards-Oriented Event-Triggered Load Frequency Control for Power Systems Under Limited Communication Bandwidth. *IEEE Trans. Control Syst. Technol.* 30 (2), 860–868. doi:10.1109/tcst.2021.3070861

Sun, Y., (2023). Stability Analysis of Load Frequency Control for Power Systems With Interval Time-varying Delays. *Front. Energy Res.* 10. doi:10.3389/fenrg.2022.1008860

Tang, J., Liu, G., and Pan, Q. (2021). A Review on Representative Swarm Intelligence Algorithms for Solving Optimization Problems: Applications and Trends. *IEEE/CAA J. Autom. Sinica* 8 (10), 1627–1643. doi:10.1109/jas.2021.1004129

Tsai, H.-C., and Lin, Y.-H. (2011). Modification of the Fish Swarm Algorithm With Particle Swarm Optimization Formulation and Communication Behavior. *Appl. Soft Comput.* 11 (8), 5367–5374. doi:10.1016/j.asoc.2011.05.022

Veerasamy, V., (2020). A Hankel Matrix Based Reduced Order Model for Stability Analysis of Hybrid Power System Using PSO-GSA Optimized Cascade PI-PD Controller for Automatic Load Frequency Control. *IEEE Access* 8, 71422–71446. doi:10.1109/access.2020.2987387

Wang, X., (2022). A Data-Driven Uncertainty Quantification Method for Stochastic Economic Dispatch. *IEEE Trans. Power Syst.* 37 (1), 812–815. doi:10.1109/tpwrs.2021.3114083

Wen, S., (2016). Event-Triggering Load Frequency Control for Multiarea Power Systems With Communication Delays. *IEEE Trans. Ind. Electron.* 63 (2), 1308–1317. doi:10.1109/tie.2015.2399394

Wu, Z.-G., (2018). Event-Triggered Control for Consensus Problem in Multi-Agent Systems With Quantized Relative State Measurements and External

Disturbance. *IEEE Trans. Circuits Syst. I Regul. Pap.* 65 (7), 2232–2242. doi:10.1109/tcsi.2017.2777504

Wu, Z., (2020). Adaptive Event-Triggered Observer-Based Output Feedback $\mathcal L_{\infty }$ Load Frequency Control for Networked Power SystemsL∞Load Frequency Control for Networked Power Systems. *IEEE Trans. Ind. Inf.* 16 (6), 3952–3962. doi:10.1109/tii.2019.2942637

Yan, C.-H., (2022). Stabilization of Load Frequency Control System via Event-Triggered Intermittent Control. *IEEE Trans. Circuits Syst. II Express Briefs* 69 (12), 4934–4938. doi:10.1109/tcsii.2022.3197460

Yang, D., (2020). Inertia - Adaptive Model Predictive Control-based Load Frequency Control for Interconnected Power Systems With Wind Power. *IET Gener. Transm. Distrib.* 14 (22), 5029–5036. doi:10.1049/iet-gtd.2020.0018

Yang, L., (2022). Indirect Multi-Energy Transactions of Energy Internet with Deep Reinforcement Learning Approach. *IEEE Trans. Power Syst.* 37 (5), 4067–4077. doi:10.1109/tpwrs.2022.3142969

Yuan, G., and Yang, W. (2019). Study on Optimization of Economic Dispatching of Electric Power System Based on Hybrid Intelligent Algorithms (PSO and AFSA). *Energy* 183, 926–935. doi:10.1016/j.energy.2019.07.008

Yuan, Z.-L., (2021). Delay-dependent Stability Analysis of Load Frequency Control for Power System With EV Aggregator. *Front. Energy Res.* 9. doi:10.3389/fenrg.2021.771465

Yue, D., Tian, E., and Han, Q.-L. (2013). A Delay System Method for Designing Event-Triggered Controllers of Networked Control Systems. *IEEE Trans. Autom. Contr.* 58 (2), 475–481. doi:10.1109/tac.2012.2206694

Zhang, H., Liu, J., and Xu, S. (2020). H-Infinity Load Frequency Control of Networked Power Systems via an Event-Triggered Scheme. *IEEE Trans. Ind. Electron.* 67 (8), 7104–7113. doi:10.1109/tie.2019.2939994

Zhao, X., (2022). Robust LFC of Power Systems With Wind Power Under Packet Losses and Communication Delays. *IEEE J. Emerg. Sel. Top. Power Electron.* 12 (1), 135–148. doi:10.1109/jetcas.2022.3141108

Zhou, Z., (2019). Application of Kriging Algorithm based on ACFPSO In Geomagnetic Data Interpolation. *Math. Probl. Eng.* 2019, 1–14. doi:10.1155/2019/1574918

Zhu, Y., and Gao, H. (2020). Improved Binary Artificial Fish Swarm Algorithm and Fast Constraint Processing for Large Scale Unit Commitment. *IEEE Access* 8, 152081–152092. doi:10.1109/access.2020.3015585